International Journal of Mechanical, Industrial and Aerospace Sciences
ISSN: 2517-9950
Vol:8, No:7, 2014

# Jet-Stream Airsail: Study of the Shape and the Behavior of the Connecting Cable

Christopher Frank, Yoshiki Miyairi

*Abstract*—A Jet-stream airsail concept takes advantage of aerology in order to fly without propulsion. Weather phenomena, especially jet streams, are relatively permanent high winds blowing from west to east, located at average altitudes and latitudes in both hemispheres. To continuously extract energy from the jet-stream, the system is composed of a propelled plane and a wind turbine interconnected by a cable. This work presents the aerodynamic characteristics and the behavior of the cable that links the two subsystems and transmits energy from the turbine to the aircraft. Two ways of solving this problem are explored: numerically and analytically. After obtaining the optimal shape of the cross-section of the cable, its behavior is analyzed as a 2D problem solved numerically and analytically. Finally, a 3D extension could be considered by adding lateral forces. The results of this work can be further used in the design process of the overall system: aircraft-turbine.

*Keywords*—Jet-stream, cable, tether, aerodynamics, aircraft, airsail, wind.

## I. Introduction

SINCE its origin, aviation has found a powerful source of inspiration in nature observation. Indeed, Leonardo da Vinci, an Italian Renaissance engineer and inventor drew detailed plans of a series of flying machines based on the flight of birds. More recently, famous pioneers such as Clément Ader observed how birds are making profit of wind and gusts so as to fly effortless and cover long distances [1]. From these observations, he concluded that flight had to exploit aerology. This is done, in particular, by modifying the wing's shape during the flight. This idea has been applied to Ader's first plane Eole: it was fitted with six handles to adapt the airfoil geometry (camber, twist, surface and position). However, the analogy with birds did not include wing flapping, since Ader had directly opted for the "glider + propeller" formula which has proven full of future! Aviation development has moved away over time from its original nature-based inspiration. As a consequence of the increase of flight speed, planes have become more and more rigid and are equipped with hinged control surfaces instead of flexible wings. Even if sailplanes are not meant to look like birds, they exploit the potential of "free flight" offered by atmospheric phenomena. However, gliding is a sport involving a relatively small number of enthusiasts: it is far from commercial aviation which we are interested in.

C. Frank is with the Department of Aerospace Engineering, Georgia Institute of Technology, Atlanta, GA, 30332 USA (e-mail: christopher.frank@gatech.edu).
Y. Miyairi is with the Department of Aerospace Engineering, Georgia Institute of Technology, Atlanta, GA, 30332 USA (e-mail: ymiyairi3@gatech.edu).

The idea of this project is to take advantage of aerology in order to fly without propulsion, but on a scale well above gliding in terms of both flight frequency and travel distance. Weather phenomena that can make it possible are jet streams which are relatively permanent high winds blowing from west to east, located at average altitudes and latitudes in both hemispheres. As a sailing boat (foil and drift/keel), a plane can extract energy from high winds. Thus, it can travel long distances by taking advantage of a wind gradient between two different altitudes. As a sailing boat, it is also quite possible to fly different courses with respect to the wind (from tailwind to headwind), and go much faster than the wind in favorable conditions. Thus, in addition to crossing long distances using only energy from the jet-stream, it is conceivable to achieve it at relatively high speeds.

In order to continuously extract energy from the jet-stream, the system will be composed of two sub-systems interconnected by a cable: one inside the jet-stream, the other outside. The wind difference is the cornerstone to get a positive propulsive balance for the system. A plane with a propeller is linked to a subsystem containing a wind turbine providing the necessary energy. This system can work if the turbine faces a faster airflow than the propeller (e.g. plane flying downwind in the jet-stream, turbine outside) and if the efficiencies are high enough to allow energy transmission from the turbine to the propeller.

As presented on Fig. 1, the two subsystems are linked by a cable that can have a length of several hundreds of meters. Therefore, its behavior must be taken into account for the design and the feasibility study of the concept.

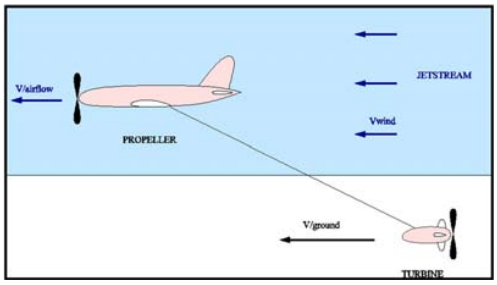


Fig. 1. Principle of the concept [2]

Jet-stream exploitation to propel planes is not a completely new idea. Delft University has been working on the design of an aircraft capable of flying around the world on solar and wind energy: they have come up with the notion further

developed in this project of using two interconnected planes, one of them flying inside the jet-stream. The French Aerospace Laboratory (ONERA) is also working on the feasibility of such concepts [2]. In order to precisely design the two subsystems and the cable, a detailed study of the behavior of the cable is essential. Since the idea of linking two aircraft by a several-kilometer cable is new and innovative, no experimental data or information are available. Therefore, one of the most challenging part of the design remains in the characterization of the cable in terms of behavior, shape and drag generated. This part will be tackled in this project.

Firstly, the drag coefficient of the cable must be modeled based on the cross-section. Once it has been done, an optimization is performed in order to find the best aerodynamic configuration. In order to find the drag along the cable, the wind gradient must be modeled by studying the jet-stream's characteristics. Secondly, different methods of calculation are used to compute the shape of the cable and the results are checked with simple and well-known cases. Finally, lateral forces are considered, implying a 3D matrix analysis.

## II. Review of Previous Work

As previously mentioned, jet-stream exploitation for propel planes is not a completely new idea. So far, several approaches have already been investigated: a linked gliders concept, a propeller-turbine concept, a dynamic flight through horizontal wind gradient, etc. One of the most famous concepts is the airplane powered by an engine, which is fed by a towing line (tether) linked to a turbine.

The most crucial challenge in the former type of projects such as CONDOR from Boeing [3], [4], [5] (Fig. 2), and Perseus from NASA/Aurora Flight Sciences [6], [7] is to use glider type of aircraft which are powered by engines. Especially, the key factor of these projects is to develop engines that can provide enough thrust even if the aircraft fly at high altitude (the ceiling of CONDOR is 67,000 ft).

Fig. 2. The airplane of CONDOR-High Altitude Long Endurance (HALE) project [3]

Moreover, the latter type of research such as Stratospheric Towing Project (STRATOW) [8], [9] is mainly focused on researching the characteristics and the shape of towing line. As presented on Fig. 3, the two airplanes are linked by a cable that can measure up to several hundreds of meters because large wind gradients are required between them. STRATOW concept, i.e. towing a glider as a kite, becomes feasible thanks to the development of new materials with extreme strength as well as very thin tethers.

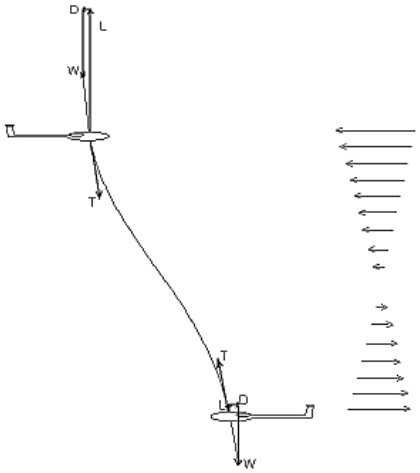


Fig. 3. The concept of STRATOW [10]

In addition, a numerical model is also presented by some researchers such as Melkert [11] describing the forces on the cable and the resulting shape, considering the flight conditions of the airplane. Besides, simplified models can be developed using several approximations. Thanks to these analytical models, the dependence of parameters such as cable diameter and aircraft speed can be characterized. Especially, the analytic form plays an important role to validate the numerical results. Nevertheless, these models are usually based on very simplifying assumptions and there is a lack of models including a large number of parameters such as wind gradients and airfoil-shaped cables.

## III. Aerodynamic Characteristics of the Cable

Before determining the behavior and the shape of the cable, it is important to identify the corresponding requirements. Two main functions can be identified: the mechanical link between the two subsystems and the energy transfer from the turbine to the aircraft. The material used for each function is different. The mechanical function tends to be met by using light and strong materials such as carbon fibers and high-modulus polyethylene (used for gliders). The electric function can be met by conducting materials such as cooper.

### A. Cylindric Cable with a Circular Cross-Section

Using experimental data from Pierre Rebuffet [12], one can mathematically model the curve which provides the drag coefficient of a cylinder with a circular cross-section as a function of the Reynolds number. Since no simple physics-based model or interpolation function provides an accurate model over the entire range, the following methodology is used to approximate the curve:

1) Creation of two vectors of points which are located on the curve (X-axis and Y-axis)

2) Separation of the curve in different intervals
3) Mathematical interpolation using `cftool` from `Matlab`
4) Conversion of the function from the dB-scale to the real scale

The results of the interpolation as well as the real function are presented on Fig. 4. As shown, the two curves are almost confounded, and therefore the approximation is considered to be accurate enough for this study.

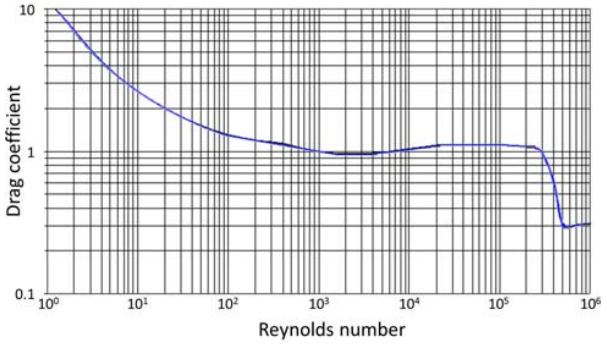


Fig. 4. Comparison between the interpolation and the real curve

The Reynolds number which appears in this project is between $10^3$ and $5.10^5$. Therefore, the value of the drag coefficient is close to 1 and consequently very high. Indeed, a NACA 0012 airfoil with a height of 5 mm generates 12 times less drag than a circular cable with a diameter of 5 mm. Thus, it would be profitable to streamline the cable.

### *B. Airfoil-Shaped Cable*

Rapid electric estimations demonstrate that the required cable diameter is relatively small. Therefore, one can streamline the fibers for energy transmission around the circular section. An idea is to streamline them according to an airfoil shape. Several solutions are imagined and the two most practical and efficient are presented hereafter.

*1) Rectangular cross-section:* The idea is to keep a rectangular cable as presented on Fig. 5 and to streamline it in order to reduce the drag. The goal of this part is to find the optimum configuration and its benefits on the drag.

The equation of the extrados of the airfoil is given by the function $f$ and the other notations are presented on Fig. 5. First, one can notice that the definition of $f$ provides (1).

$$x_A = f^{-1}\left(\frac{E}{2}\right) \tag{1}$$

In the case of a NACA airfoil with a relative thickness $\epsilon$, $f$ is described by (2) found in Jack Moran's book [13].

$$f(x) = \epsilon c\left(0.2969\sqrt{\frac{x}{c}} - 0.126\frac{x}{c} - 0.3516\left(\frac{x}{c}\right)^2 + 0.2843\left(\frac{x}{c}\right)^3 - 0.1015\left(\frac{x}{c}\right)^4\right) \tag{2}$$

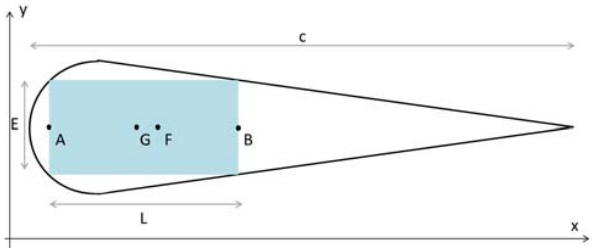


Fig. 5. Rectangular cross section within the airfoil

Since the aerodynamic center is approximately at 25% of the chord of the airfoil, the center of mass must be located in front of it so that the airfoil remains statically stable. Nevertheless, 20% of the chord is selected to keep a safety margin. It can be mathematically described by (3).

$$c = 5\left(x_A + \frac{L}{2}\right) \tag{3}$$

Considering the drag coefficient of a symmetric NACA airfoil $C_D$, the drag is computed by (4).

$$D = \frac{1}{2}\rho S V^2 \frac{0.1134}{Re^{0.2}} \tag{4}$$

Fig. 6 represents the drag as a function of the relative thickness. As shown, there is an optimum for the relative thickness at $\epsilon = 0.27$.

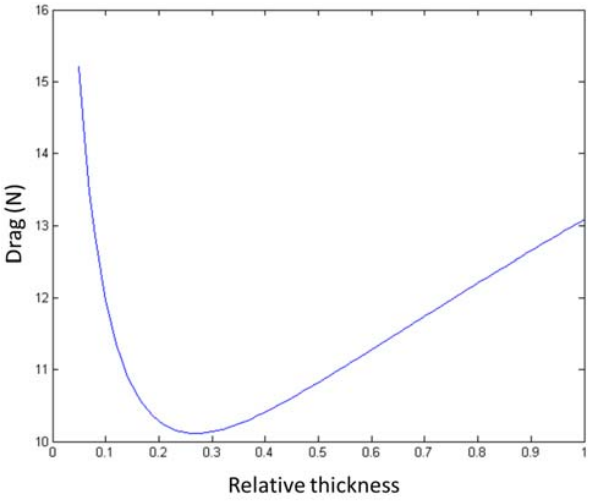


Fig. 6. Computed drag as a function of the relative thickness

Using this configuration, Fig. 7 displays the shape of both the airfoil and the cable.

*2) Streamlined cable:* In this section, the cable goes until the leading edge of the airfoil and is streamlined in order to decrease the drag even more. The surface of the airfoil in front of the rectangle from Fig. 8 is called $S_{BA}$ and the center of mass of the latter is called $x_{G_{BA}}$. The conservation of the different areas provides (5).

$$S_{BA} + \epsilon\left(x_B - x_A\right)^2 = S_{tot} \tag{5}$$

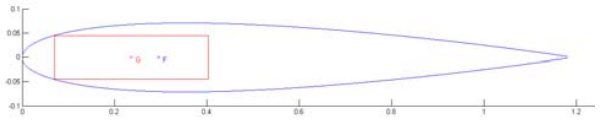

Fig. 7. Rectangular cable within a NACA airfoil

By constraining the center of mass to be at 20% of the chord, (6) is provided:

$$S_{BA}x_{G_{BA}}(x_A) + (S_{tot} - S_{BA}(x_A))\,\frac{x_B + x_A}{2} = 0.2\,c\,S_{tot} \tag{6}$$

Equation (7) provides the relationship between the relative thickness $\epsilon$ and the location of the points A and B.

$$\epsilon = \frac{2f(x_A)}{x_B - x_A} \tag{7}$$

Finally, the location of the center of mass can be expressed by (8).

$$x_{G_{BA}} = \frac{2}{S_{BA}} \int_0^{x_A} x f(x) dx \tag{8}$$

The parametric `Matlab` tool enables the plot of the airfoil and the cable. An example is given on Fig. 8.

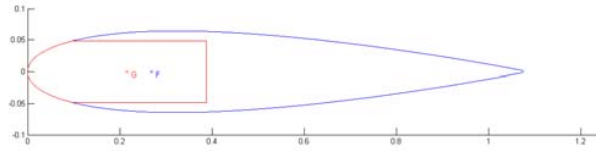

Fig. 8. Rectangular cable within a NACA airfoil with full leading edge

### C. Effects of the Relative Thickness

Based on Nathalie Bivaud's work [14] and using a new and more precise interpolation model, one can determine a parametric drag coefficient of a symmetric NACA airfoil. Data from R. Sheldahl and P. Klimes [15] are also used. The drag coefficient can be written as a function of three constants $a$, $b$ and $c$ as defined by (9).

$$C_D = a.Re^b + c \tag{9}$$

Those three coefficients only depend on the relative thickness $\epsilon$ and their expressions are provided by (10), (11) and (12).

$$a = 0.0003515\epsilon^4 - 0.02859\epsilon^3 + 0.8785\epsilon^2 - 12.191\epsilon + 69.82 \tag{10}$$

$$b = 3.364.10^{-5}\epsilon^3 - 0.002318\epsilon^2 + 0.05664\epsilon - 1.013 \tag{11}$$

$$c = 0.0001\epsilon + 0.0038 \tag{12}$$

### D. Results

An optimization with `Matlab` has been used in order to find the best relative thickness: $\bar{\epsilon} = 12.5\%$ when the rear of the rectangular cable is in contact with the border of the airfoil. Fig. 9 shows the drag per unit length generated as a function of the relative thickness for nominal conditions.

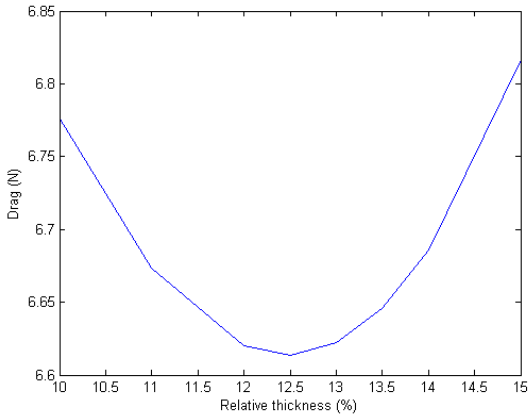


Fig. 9. Evolution of drag with respect to the relative thickness of the airfoil

It allows a very elongated airfoil with a reduced drag. Finally, another configuration is also studied: a cable which fills the front of the airfoil. In this case, the manufacturing of the cable would probably be more difficult since the cable follows the exact shape of the airfoil from its leading edge to the rear of the cable. There is no more "straight line" curve. The results are presented in Table I. It appears that the optimum is given by a cable which fills the front of the airfoil. Moreover, even a simple fairing would considerably reduce the drag (divided by at least 10).

TABLE I
COMPARISON OF UNITARY DRAG FOR DIFFERENT CONFIGURATIONS

| Type of cross-section | Drag (N) |
|---|---|
| Circular | 95.55 |
| Rectangular cable within airfoil | 8.18 |
| Rectangular cable within airfoil with streamlined leading edge | 6.62 |
| Full leading edge | 6.61 |

## IV. MODELING OF THE JET-STREAM

In order to determine the drag of the cable, the relative speed between the wind and the cable must be determined. Moving with the whole system, only the speed of the wind can be considered. Using the data from Météo France (the French national meteorological service), the speed of the wind is plotted as a function of altitude and season on Fig. 10. Therefore, a piecewise approximation is computed and presented in Table II. In these formulas, the altitude $h$ is in meters.

TABLE II
PIECEWISE APPROXIMATION OF THE RELATIVE JET-STREAM WIND FOR NORTHERN HEMISPHERE

| Season | $h \leq 12$ km | $h \geq 12$ km |
|---|---|---|
| Summer | $V = 0.0038h - 2.2015$ | $V = -0.0037h + 86.56$ |
| Winter | $V = 0.0017h + 0.8969$ | $V = -0.0029h + 56.476$ |

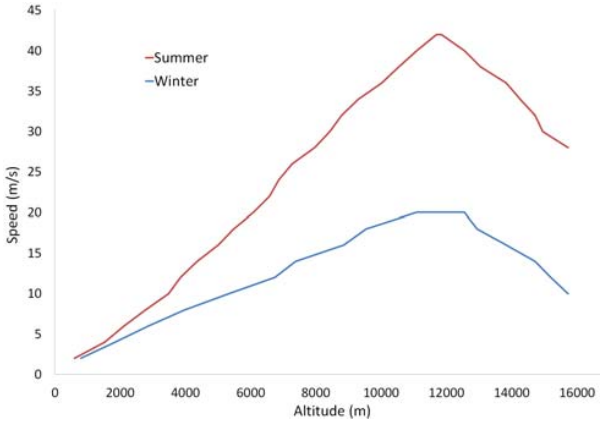


Fig. 10. Wind profile as a function of altitude

## V. Numerical Computation of the Shape of the Cable

### A. Principle

In order to numerically solve the problem, the cable is discretized in small straight pieces on which the Newton's second law is applied. The different parameters taken into account are: the variation of the density along the cable with altitude, the variation of the drag coefficient, the drag with the speed, and the variation of the speed due to the wind gradient along the cable. Nevertheless, the drag due to the tangential component of the speed is neglected. Therefore, only the normal component of the drag is taken into account for the drag computation: $V_n = V \sin\theta$.

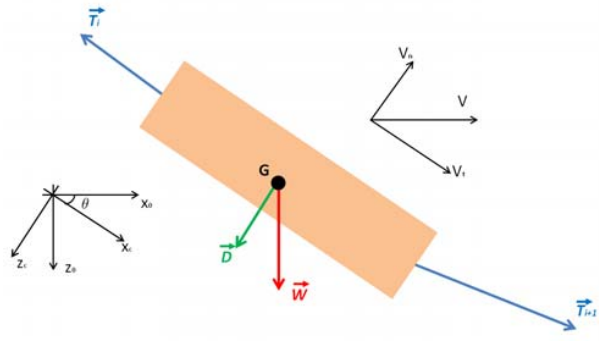


Fig. 11. Equilibrium of a small piece of the discretized cable

As displayed in Fig. 11, $\theta$ is the angle between the horizontal and the direction of the cable. If the turbine is above the aircraft, $\theta_0$ is negative and if the turbine is below the aircraft, this angle is positive. Two different reference frames are implemented. The first one, called $R_0$, corresponds to the Earth-Surface Earth-Fixed (ESEF) reference frame and is considered as the inertial reference frame. $\overrightarrow{x_0}$ is the horizontal axis in the direction of the aircraft speed. Considering a constant speed and constant altitude cruise, $\overrightarrow{V}$ is parallel to $\overrightarrow{x_0}$. $\overrightarrow{z_0}$ corresponds to the downward vertical. The second one, called $R_c$ is linked to the cable. A rotation of $\theta$ around the Y-axis transforms $R_0$ to $R_c$.

To perform the calculation, the principle is to start from two boundary conditions: the tension $T_0$ and the angle $\theta_0$ at the turbine. To find those parameters, the equilibrium of the turbine should be considered. Thus, by considering the boundary conditions at one end of the cable, it is possible to go to the other end by applying the second Newton's law on each piece of the discretized cable. Moreover, it is assumed that the direction of the cable is parallel to the resultant of the forces acting at the boundary of the first piece.

The equilibrium of the forces which is propagated throughout the cable provides the expression of the tension (magnitude and direction) at the other end. Equations (13), (14) and (15) provide the required expressions for the equilibrium computation.

$$\overrightarrow{W} = \rho_c \left(\frac{\pi d^2}{4}\right) dl\, g\, \overrightarrow{z_0} \tag{13}$$

$$\overrightarrow{D} = D\overrightarrow{z_c} = -\frac{1}{2}\rho\, d\, dl \left(V^2 \sin\theta \sin|\theta|\right) C_x\, \overrightarrow{z_c} \tag{14}$$

$$\overrightarrow{T}_i = T_i\, \overrightarrow{x_c} = T_i \cos\theta\, \overrightarrow{x_0} - T_i \sin\theta\, \overrightarrow{z_0} \tag{15}$$

In the numerical computation, the unknown is $\overrightarrow{T_{i+1}}$ (Fig. 11). Moreover, the expression of the drag seems unusual but it is needed to make the resolution as generic as possible. The idea is based on the fact that the drag must be in the same direction as the normal velocity. Thus, the use of absolute value on one of the sin function provides the right direction to the drag with respect to $\overrightarrow{z_c}$. This drag is then expressed in the ESEF reference frame as shown in (16).

$$\overrightarrow{D} = D\sin\theta\overrightarrow{x_0} + D\cos\theta\overrightarrow{z_0} \tag{16}$$

On the one hand, when the turbine is above the aircraft, $\theta$ is negative and therefore, the drag has a downward component. On the other hand, when the turbine is below the aircraft, $\theta$ is positive and therefore, the drag has an upward component.

### B. Iterations

From the known boundary conditions at the turbine $\overrightarrow{T_0}$, the equilibrium provides $\overrightarrow{T_1}$, $\overrightarrow{T_2}$, etc. The goal is to link the two subsystems with a given altitude difference. The latter is computed in order to benefit from a sufficient wind gradient due to the jet-stream. Consequently, the shutoff parameter is based on the altitude. Nevertheless, another security criterion must be implemented for the impossible cases. Thus, a maximum length for the cable is considered.

At the end of the simulation, the sizing parameters can be extracted:

- $(T_f, \theta_f)$: magnitude and angle of the tension applied to the aircraft
- $T_{max}$: maximal tension in the cable

In order to take into account the diameter of the cable, another loop is created based on the new diameter found by (17). $d$ is the diameter of the cable, $T$ the tension and $\sigma_{adm}$ the maximum admissible constraint for the cable.

$$d = 2\sqrt{\frac{T}{\pi\sigma_{adm}}} \tag{17}$$

### C. Results

Fig. 12 displays the results for different starting angles and different magnitudes when the turbine is above the aircraft. The higher the magnitude of the tension is, the darker the color is. One can notice that for higher tension, the cable becomes smaller and therefore lighter. Nevertheless, it requires a high lift from the subsystem which is above. Besides, the closer the angle is from the horizontal, the longer the cable becomes so that it is profitable to start from a cable with an initial angle close to the vertical. However, on a flight dynamic point of view, this choice implies a good lift-to-drag ratio for the turbine.

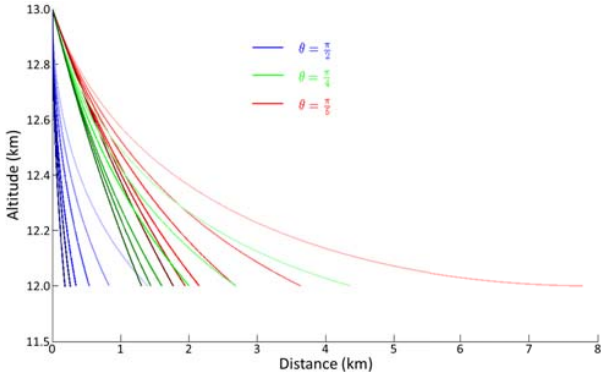


Fig. 12. Results of the simulation

When the turbine is above the aircraft, impossible cases can appear. Indeed, the combination of a low angle (close to the horizontal) and a low tension within the cable could prevent the cable to reach the required altitude difference. On Fig. 13, one can observe that the faster the aircraft is flying, the longer the cable is and thus the higher the tension is. For high speed, the drag becomes even more predominant than the weight of the cable. Therefore, the cable tends to be longer and the two aircraft farther.

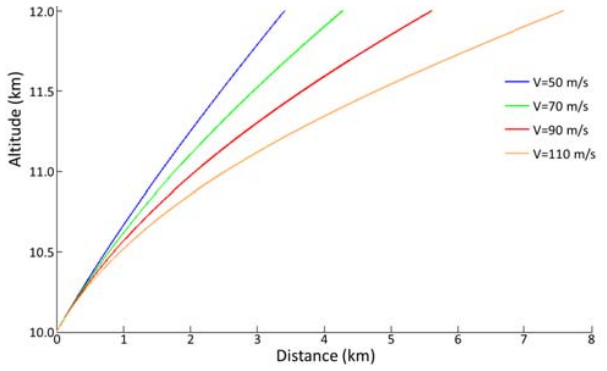


Fig. 13. Impact of the aircraft speed on the shape of the cable

Fig. 14 presents the results when the turbine is 500 meters above the aircraft and the initial tension is equal to 50 kN. Looking at the different shapes, it appears that there exists a maximum cross-section for the cable after which the case becomes impossible. This limit is reached when the angle between the cable and the horizontal goes towards zero at the bottom end of the cable.

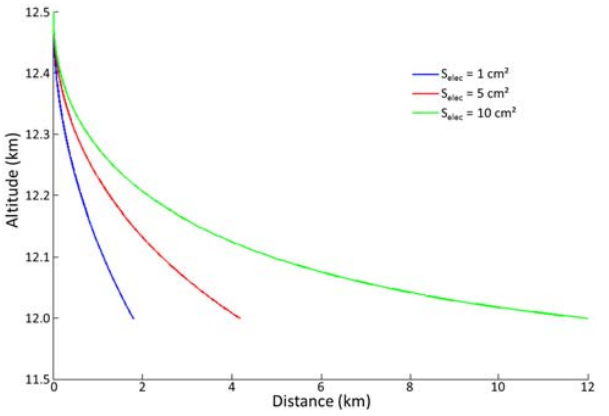


Fig. 14. Impact of the cable's cross-section on the shape of the streamlined cable

## VI. Validation of the Numerical Model

Even if the previous observations seem to be physically coherent, it is important to validate them by comparing the numerical solution with known and simple analytical solutions.

### A. Comparison with the Massless Cable

*1) Assumptions:* Wubbo Ockels [16] already developed a set of assumptions to simply and analytically solve this problem. In this resolution, the weight of the cable is assumed to be negligible, the drag coefficient is set as a constant equal to one and the speed is assumed to be constant over the entire cable. A rapid study shows the validity domain of the main assumption: a negligible weight. Thus, the ratio $D/W$ is evaluated in (18).

$$\frac{D}{W} = \frac{\frac{1}{2}\rho\, d\, dl\, (V\sin\theta)^2\, C_x}{\rho_c \left(\frac{\pi d^2}{4}\right) dl\, g} = \frac{2\rho C_x V^2 \sin^2\theta}{g\rho_c \pi d} \qquad (18)$$

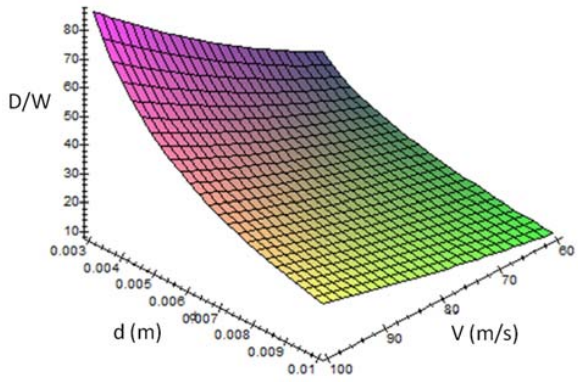


Fig. 15. Ratio drag over weight with respect to the effective speed and the diameter of the cable

In order to evaluate this ratio, the following approximations are made:

- $C_x$ = 1
- $\rho_c$ = 1,053 kg/m$^3$ for a carbon cable
- $\rho$ = 0.42 kg/m$^3$ at an altitude equal to 10 km

Finally, the ratio $D/W$ is plotted for different values of $V \sin\theta$ and $d$ on Fig. 15. One can conclude that for speeds higher than 70 m/s and for reasonably small diameters, the ratio rapidly goes over 20-30 so that the weight could be negligible compared to the drag. Nevertheless, when the cable has a small angle of incidence, the effective speed would be small and this assumption might become wrong.

*2) Derivation of the equations:* Considering a small piece of cable and the definition of $\theta$, a small variation of altitude can be written as $dh = dl \sin\theta$. Moreover, a small variation of tension can be related to a small variation of angle by the formula: $dT = Td\theta$. Thus, the differential equation is described by (19).

$$\frac{d\theta}{sin\theta} = \frac{\frac{1}{2}\rho C_x dV^2 dh}{T} \tag{19}$$

The right hand side of (19) can be easily integrated by modeling the density by the common exponential model described by (20) with $\rho_0$ = 1.225 kg/m$^3$ and $H_p$ = 9000 m.

$$\rho = \rho_0 e^{-\frac{h}{H_p}} \tag{20}$$

The left hand side of (19) can be integrated by setting $\theta = 2\alpha$ as shown by (21).

$$\int_{\theta_1}^{\theta_2} \frac{d\theta}{\sin\theta} = 2\int_{2\alpha_1}^{2\alpha_2} \frac{d\alpha}{\sin 2\alpha} = \int_{2\alpha_1}^{2\alpha_2} \frac{d\alpha}{\sin\alpha\cos\alpha} = \int_{2\alpha_1}^{2\alpha_2} \frac{\cos\alpha d\alpha}{\sin\alpha\cos^2\alpha} = \int_{2\alpha_1}^{2\alpha_2} \frac{\tan'\alpha d\alpha}{\tan\alpha} = \left[\ln\left(\tan\frac{\theta}{2}\right)\right]_{\theta_1}^{\theta_2} = \ln\left(\tan\frac{\theta_2}{2}\right) - \ln\left(\tan\frac{\theta_1}{2}\right) \tag{21}$$

Finally, (22) presents the tension of the cable as a function of the altitudes of the two subsystems and the angle between the end points of the cable and each subsystem.

$$T = \frac{\frac{1}{2}\rho_0 C_x dV^2 \left(e^{-\frac{h_1}{H_p}} - e^{-\frac{h_2}{H_p}}\right)}{\ln\left(\tan\frac{\theta_2}{2}\right) - \ln\left(\tan\frac{\theta_1}{2}\right)} \tag{22}$$

Therefore, there is an analytical expression that links the three following important parameters:

- The angle between the cable and the lower subsystem $\theta_1$
- The angle between the cable and the upper subsystem $\theta_2$
- The tension $T$ within the cable

Assuming two of the three previous parameters as known, it is possible to find the last one. Usually, the conditions at the turbine are known as well as the tension throughout the cable.

*3) Application:* Considering a nominal case, the numerical solution is compared with the analytical solution. As assumed for the formula, the massless cable is characterized by a density of 0 kg/m$^3$ and the speed is constant along the cable. The parameters are:

- V = 50 m/s
- Altitude turbine = 12 km
- Altitude aircraft = 10 km
- $T_0$ = 4 kN
- $\theta_2$ = 72°
- Cable diameter = 5 mm
- $C_x$ = 1
- $\rho_e$ = 0

Using (22), the unknown $\theta_1$ can be expressed by a single equation presented by (23). Moreover, the numerical result for the aforementioned conditions is also provided.

$$\theta_1 = 2\times \arctan\left(\exp\left[\ln\left(\tan\frac{\theta_2}{2}\right) - \frac{\frac{1}{2}\rho_0 C_x dV^2\left(e^{-\frac{h_1}{H_p}} - e^{-\frac{h_2}{H_p}}\right)}{T}\right]\right) = 26.4165° \tag{23}$$

Using the numerical computation, the final angle is equal to $\theta_1 = 26.4133$ which corresponds to a relative error around 0.01%. Moreover, the final shape of the cable is presented on Fig. 16.

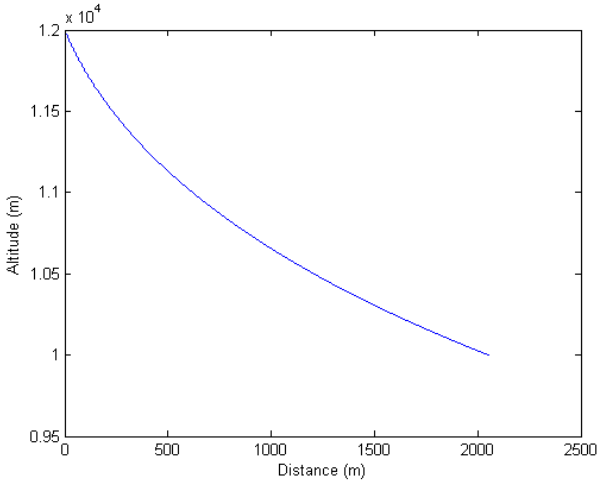


Fig. 16. Shape of the massless cable for nominal conditions

*4) Improvement of the model:* Using the previous model of the jet-stream, the previous modeling can be improved by implementing the altitude variable into the speed due to the wind gradient. Thus, the speed becomes $V = V_{AC} + a_V(h_a - h)$ and (22) can be replaced by (24).

$$T = \frac{\frac{1}{2}\rho_0 C_x d H_p}{\ln\left(\tan\frac{\theta_2}{2}\right) - \ln\left(\tan\frac{\theta_1}{2}\right)} \times \left(\left[(V_{AC} + a_v h_a - a_v h_1)^2 + 2H_p a_V\left(a_v h_1 - V_{AC} - a_v h_a + a_v H_p\right)\right]\exp\left(-\frac{h_1}{H_p}\right) - \left[(V_{AC} + a_v h_a - a_v h_2)^2 + 2H_p a_V\left(a_v h_2 - V_{AC} - a_v h_a + a_v H_p\right)\right]\exp\left(-\frac{h_2}{H_p}\right)\right) \quad (24)$$

### B. Comparison with the Catenary

Another well-known problem with an analytical solution is the catenary. Analyzing the equation of the cable presented on Fig. 17 would allow us to validate the accuracy of this model.

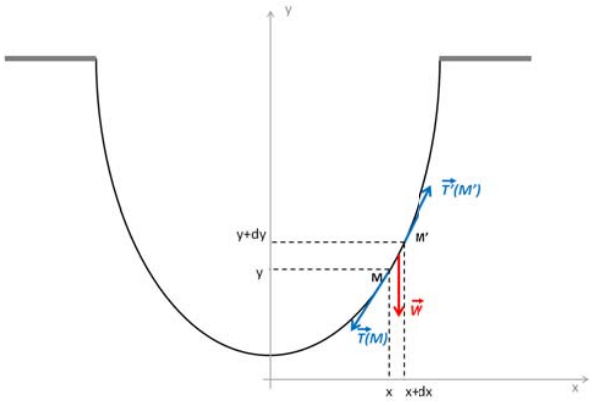


Fig. 17. Configuration of the catenary

Using the notations from Fig. 17, a small piece of the cable has a length equal to $dl = dx\sqrt{1+y'(x)^2}$. The Newton's second law provides (25).

$$\vec{T}'(M') + \vec{T}(M) + \rho\frac{\pi d^2}{4} g dl \times (-\vec{u_y}) = \vec{0} \quad (25)$$

Moreover, $T'_x(M) = T'_x(M') = T_0$ where $T_0$ is a positive constant. Using the same argument on the Y-axis, (26) is written.

$$\frac{T'_y(M)}{T_0} - \frac{T'_y(M')}{T_0} - \frac{\rho\frac{\pi d^2}{4} g dl}{T_0} = 0 \quad (26)$$

Assuming that the tension is parallel to the cable:

$$y'(x+dx) - y'(x) = \frac{\rho\frac{\pi d^2}{4} g}{T_0} dx\sqrt{1+y'(x)^2}$$

Finally, the differential equation is given by (27).

$$\frac{d^2y}{dx} = \frac{\rho\pi d^2 g}{4T_0}\sqrt{1+y'(x)^2} \quad (27)$$

Using $y'(x) = \sinh(u(x))$, one can obtained $y''(x) = u'(x)\cosh(u(x)) = \frac{\rho\pi d^2 g}{4T_0}\cosh(u(x))$. The boundary condition is given by $y'(0) = 0$ due to symmetry and therefore the solution is provided by (28).

$$y(x) = \frac{4T_0}{\rho\pi d^2 g}\cosh\left(\frac{\rho\pi d^2 g}{4T_0}x\right) + \lambda \quad (28)$$

This analytical form is plotted in red on Fig. 18 against the previous numerical solution in blue for nominal conditions. As observed, the two solutions seem to be very close so that the two curves are confounded. The relative error between the two solutions is around $10^{-3}\%$. Thus, the numerical model is satisfying for those conditions.

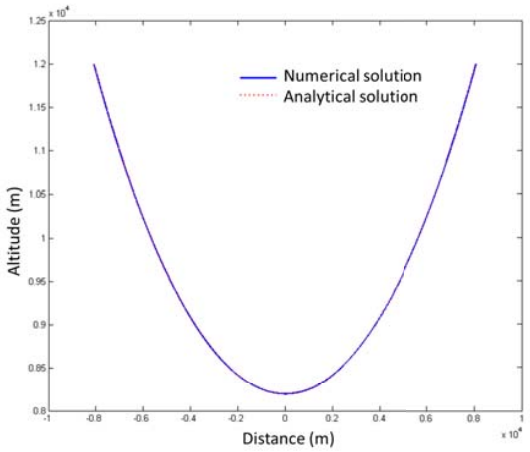


Fig. 18. Comparison between the analytical solution and the numerical computation for the catenary

### C. Convergence Study

The convergence of the model can also be studied by plotting the relative error concerning the final angle and the final tension with respect to the size of the system (Fig. 19). As expected, the accuracy decreases with the size of the pieces, but even for long pieces, the relative error remains within acceptable limits.

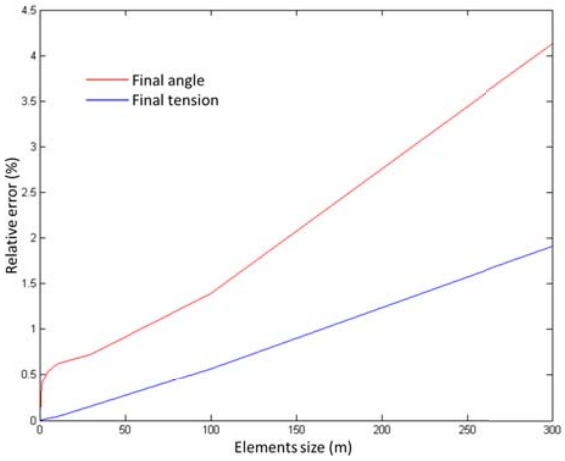


Fig. 19. Relative error vs. elements size

## VII. Sensitivity analysis of the parameters and simplifications

A complete analytical resolution seems impossible because of the complexity of the equations and the interrelationships between the different forces. Nevertheless, several simplifications could be made without reducing the precision and the accuracy of the simulation.

### A. Wind gradient

The wind gradient due to the atmospheric stream is assumed to be negligible for the drag computation. Thus, by considering an averaged relative speed, many configurations were tried and the maximal relative error found was lower than 1%. Therefore, an averaged relative speed $V_m$ is defined by (29).

$$V_m = \frac{1}{2}\left(2V_{AC} + a_V\left(h_a - h_t\right)\right) \tag{29}$$

### B. Density

As well as the wind gradient, the density of the air varies with altitude. This variation causes the variation in drag along the cable. By assuming this density constant and equal to its value at the altitude between the two subsystems, the maximal relative error never goes above 4% for very light and long cables. Therefore, an averaged density $\rho_m$ is defined by (30).

$$\rho_m = \frac{\rho_0}{2}\left(\exp^{-\frac{h_a}{H_p}} + \exp^{-\frac{h_t}{H_p}}\right) \tag{30}$$

### C. Drag Coefficient

*1) Cylindrical cable with circular cross-section:* For applications similar to the one in this project, the Reynolds number can be considered as being between $10^3$ and $5.10^5$. Therefore, in this range, the drag coefficient can be considered as a constant equal to:

$$C_{xm} = 1.05$$

*2) Cylindrical cable with streamlined cross-section:* Since the aerodynamic optimum was found for a relative thickness equal to 12.5%, the drag coefficient can be modeled by:

$$C_{xm} = 7.439824\mathrm{Re}^{-0.60898} + 0.00505$$

### D. Maximal Tension

The different simulations as well as a physical analysis show that the maximum tension within the cable is experienced at the top end of the cable and is equal to $T_0$ when the turbine is above the aircraft and $T_f$ when the turbine is below the aircraft. In order to find a single expression for this tension, a mathematical trick is described by (31).

$$T_{max} = \frac{T_f}{2}\left(1 + \frac{h_a - h_t}{|h_a - h_t|}\right) + \frac{T_0}{2}\left(1 - \frac{h_a - h_t}{|h_a - h_t|}\right) \tag{31}$$

## VIII. Analytical solution

Considering the previous simplifications and assumptions, the resolution is performed in two steps. Firstly, a constant angle for the cable is considered in order to understand how the solution can be derived and secondly, a complete solution is provided.

### A. Solution with a Constant Cable Angle

The angle between the cable and the horizontal is set to $\theta_m$ and remains constant along the cable. Therefore by neglecting the tangential drag, the only force that acts in the direction of the cable is the projection of the weight. Equation (32) describes the variation in the tension.

$$\Delta T = \rho_c l \pi \frac{d^2}{4} g \sin\theta_m \tag{32}$$

Based on (32), it is obvious that, if $\theta_m$ is positive (turbine below), the tension reaches a maximum at the aircraft. The opposite is also true: if $\theta_m$ is negative (turbine above), the tension reaches a maximum at the turbine. Equation (33) sums the forces acting in a direction perpendicular to the cable. One can conclude that even if the weight always tends to lower the cable, the drag could rise or lower the cable.

$$T_m \Delta\theta = -\rho_c l \pi \frac{d^2}{4} g \cos\theta_m + \frac{1}{2}\rho_m l d V_m^2 C_{xm} \sin\theta_m \sin|\theta_m| \tag{33}$$

An eight-equation system can then be implemented in order to solve the problem:

$$\begin{cases}
\pi d^2 \sigma_{adm} = 4\left(\frac{T_f}{2}\left(1 + \frac{h_a - h_t}{|h_a - h_t|}\right)\right. \\
\qquad\qquad \left. + \frac{T_0}{2}\left(1 - \frac{h_a - h_t}{|h_a - h_t|}\right)\right) & \text{(34a)} \\
V_m = \frac{1}{2}\left(2V_{AC} + a_V\left(h_a - h_t\right)\right) & \text{(34b)} \\
\Delta T = \rho_c l \pi \frac{d^2}{4} g \sin\theta_m & \text{(34c)} \\
T_m \Delta\theta = -\rho_c l \pi \frac{d^2}{4} g \cos\theta_m \\
\qquad + \frac{1}{2}\rho_m l d V_m^2 C_{xm} \sin\theta_m \sin|\theta_m| & \text{(34d)} \\
\rho_m = \frac{\rho_0}{2}\left(\exp^{-\frac{h_a}{H_p}} + \exp^{-\frac{h_t}{H_p}}\right) & \text{(34e)} \\
l \sin\theta_m = h_a - h_t & \text{(34f)} \\
T_m = \frac{T_0 + T_f}{2} & \text{(34g)} \\
C_{xm} = 1.05 & \text{(34h)}
\end{cases}$$

Combining (34a), (34c) and (34g), the value of $T_f$ can be found and is provided by (35).

$$T_f = T_0 \frac{2\sigma_{adm} + \rho_c g (h_a - h_t)\left(1 - \frac{h_a - h_t}{|h_a - h_t|}\right)}{2\sigma_{adm} - \rho_c g (h_a - h_t)\left(1 + \frac{h_a - h_t}{|h_a - h_t|}\right)} \tag{35}$$

Once $T_f$ has been determined, (34a) provides the required diameter of the cable through (36).

$$d = \sqrt{\frac{2}{\pi\sigma_{adm}}\left(T_f\left(1+\frac{h_a-h_t}{|h_a-h_t|}\right)+T_0\left(1-\frac{h_a-h_t}{|h_a-h_t|}\right)\right)} \tag{36}$$

Moreover, (34f) provides the expression of $\cos\theta_m$ and $\sin\theta_m$ as a function of the altitudes and the length of the cable. Finally, (34b), (34d), (34e), (34g) and (34h) provide the final expression of $\theta_f$ described by (37).

$$\theta_f = \theta_0 + \frac{-\rho_c l\pi\frac{d^2}{4}g\sqrt{1-\frac{(h_a-h_t)^2}{l^2}}+\frac{1}{2}\rho_m d V_m^2 C_{xm}\frac{(h_a-h_t)|h_a-h_t|}{l}}{T_m} \tag{37}$$

### B. Complete Solution

Now, the length of the cable is no longer given and the angle no longer constant. The new system of equations is:

$$\begin{cases} \pi d^2\sigma_{adm} = 4\left(\frac{T_f}{2}\left(1+\frac{h_a-h_t}{|h_a-h_t|}\right)+\frac{T_0}{2}\left(1-\frac{h_a-h_t}{|h_a-h_t|}\right)\right) & (38a)\\ V_m = \frac{1}{2}\left(2V_{AC}+a_V\left(h_a-h_t\right)\right) & (38b)\\ dT = \rho_c dl\pi\frac{d^2}{4}g\sin\theta & (38c)\\ Td\theta = -\rho_c dl\pi\frac{d^2}{4}g\cos(-\theta) + \frac{h_a-h_t}{|h_a-h_t|}\frac{1}{2}\rho_m dl dV_m^2 C_{xm}\sin^2\theta & (38d)\\ \rho_m = \frac{\rho_0}{2}\left(\exp^{-\frac{h_a}{H_p}}+\exp^{-\frac{h_t}{H_p}}\right) & (38e)\\ dl\sin\theta = dh & (38f)\\ C_{xm} = 1.05 & (38g) \end{cases}$$

As done before, the final tension and the diameter are determined. Those two parameters only depend on the initial tension and the altitude difference. Moreover, by combining (38b) and (38c), it is possible to obtain a differential equation where the variables can be separated. The latter is provided by (39) and each member of this equation is equal to the same constant.

$$\frac{dT}{T} = \frac{\sin\theta}{\frac{2\rho_m V_m^2 C_{xm}(h_a-h_t)}{|h_a-h_t|\rho_c\pi dg}\sin^2\theta-\cos(-\theta)}d\theta \tag{39}$$

Setting $u=\cos(-\theta)$, substitution of variables can be used to get (40).

$$\ln\frac{T_f}{T_0} = \int_{\cos\theta_0}^{\cos\theta_f}\frac{-du}{\frac{2\rho_m V_m^2 C_{xm}(h_a-h_t)}{|h_a-h_t|\rho_c\pi dg}u^2+u-\frac{2\rho_m V_m^2 C_{xm}(h_a-h_t)}{|h_a-h_t|\rho_c\pi dg}} \tag{40}$$

The goal is to integrate a rational fraction with the parameter $a$ defined by (41).

$$a = \frac{2\rho_m V_m^2 C_{xm}(h_a-h_t)}{|h_a-h_t|\rho_c\pi dg} \tag{41}$$

The poles of this rational fraction are $u_1$ and $u_2$ defined by:

$$u_1 = \frac{-1+\sqrt{1+4a^2}}{2a} \qquad u_2 = \frac{-1-\sqrt{1+4a^2}}{2a}$$

Therefore, (40) can be transformed into (42).

$$\ln\frac{T_f}{T_0} = \frac{-1}{a(u_1-u_2)}\int_{\cos\theta_0}^{\cos\theta_f}\frac{1}{u-u_1}-\frac{1}{u-u_2}du = \frac{1}{a(u_1-u_2)}\left(\ln\left|\frac{\cos\theta_f-u_2}{\cos\theta_f-u_1}\right|+\ln\left|\frac{\cos\theta_0-u_1}{\cos\theta_0-u_2}\right|\right) \tag{42}$$

Thus, the final angle can be calculated but there are two solutions described by (43) and (44) because of the absolute value:

$$\theta_{f1} = \frac{h_a-h_t}{|h_a-h_t|}\times \arccos\left(\frac{u_1\exp\left(a(u_1-u_2)\ln\frac{T_f}{T_0}-\ln\left|\frac{\cos\theta_0-u_1}{\cos\theta_0-u_2}\right|\right)-u_2}{\exp\left(a(u_1-u_2)\ln\frac{T_f}{T_0}-\ln\left|\frac{\cos\theta_0-u_1}{\cos\theta_0-u_2}\right|\right)-1}\right) \tag{43}$$

$$\theta_{f2} = \frac{h_a-h_t}{|h_a-h_t|}\times \arccos\left(\frac{u_1\exp\left(a(u_1-u_2)\ln\frac{T_f}{T_0}-\ln\left|\frac{\cos\theta_0-u_1}{\cos\theta_0-u_2}\right|\right)+u_2}{\exp\left(a(u_1-u_2)\ln\frac{T_f}{T_0}-\ln\left|\frac{\cos\theta_0-u_1}{\cos\theta_0-u_2}\right|\right)+1}\right) \tag{44}$$

The choice between the two solutions must be done by numerical observations. Indeed, only one solution remains physical but it is not always the same answer. The choice that has to be made corresponds to the resolution of (45).

$$\left|\frac{\cos\theta_f-u_2}{\cos\theta_f-u_1}\right| = c^{te} = \omega \tag{45}$$

By definition, $u_2$ would always be negative when the turbine is above the aircraft and $u_1$ would always be negative when the turbine is below the aircraft. Therefore, when the aircraft is above, (46) must be solved.

$$\omega|\cos\theta_f-u_1| = \cos\theta_f-u_2 \tag{46}$$

The solution depends on the relative position of $\theta_f$ with respect to $u_2$ and cannot be predicted.

### C. Validity Domain

When the aircraft is above the turbine, the relative error on the final angle is lower than 2% for almost every case close to the nominal conditions. When the turbine is above the aircraft, the relative error is lower than 1% in almost all configurations and especially for conditions close to nominal conditions. The accuracy is improved for high initial tension, slow speed, small altitude difference and an initial angle close to the vertical. The precision on the final tension is always accurate and the error lower than 0.5%

## IX. Three-dimensional solution

### A. Problem Resolution

Other concepts of attached aircraft imply lateral forces and the calculation must be done by considering another dimension. A numerical solution can be computed using the same principle as for the two-dimensional case. Nevertheless, in this resolution, other input variables are fixed: the lateral tension, the length of the cable, and the altitude difference. By discretizing the cable, a matrix can be created in order to solve the problem. Fig. 20 shows how a matrix is used to apply the boundary conditions as well as the Newton's second law. Indeed, the latter is projected on the three axes. In this matrix, $\overrightarrow{R}$ represents the tension within the cable and $\overrightarrow{D}$ the drag. Moreover, $\Delta$ is used to compute the difference between two consecutive elements. Equation (47) defines this matrix.

$$\Delta = \begin{pmatrix} 1 & -1 & 0 & 0 & 0 & 0 \\ 0 & 1 & -1 & 0 & 0 & 0 \\ 0 & 0 & . & . & 0 & 0 \\ 0 & 0 & 0 & . & . & 0 \\ 0 & 0 & 0 & 0 & 1 & -1 \end{pmatrix} \tag{47}$$

Finally, the matrix problem can be written as shown on Fig. 20. The $n$ first lines represent the projection on the X-axis, the $n$ next lines the projection on the Y-axis and the $n$ next lines the projection on the Z-axis. Finally, the remaining rows correspond to the boundary conditions. A stretched cable is considered as initial condition and an iterative loop is created based on the tension of the cable. Therefore, at each step, $\overrightarrow{R}$ and $\overrightarrow{D}$ are computed. The loop is stopped once $\overrightarrow{R}$ has converged on a final value. In order to visualize the result, a nominal case is run and the results are presented on Fig. 21 and Fig. 22.

$$\begin{pmatrix} \Delta & 0 & 0 \\ 0 & \Delta & 0 \\ 0 & 0 & \Delta \\ & 0\,0\,\ldots\,0\,1 & \\ 0 & 0 & \frac{dl}{F_{tm}}\frac{dl}{F_{tm}}\cdots\frac{dl}{F_{tm}}\frac{dl}{F_{tm}} \\ \frac{dl}{F_{tm}}\frac{dl}{F_{tm}}\cdots\frac{dl}{F_{tm}}\frac{dl}{F_{tm}} & 0 & 0 \end{pmatrix} \begin{pmatrix} R_{x1} \\ R_{x2} \\ \ldots \\ R_{xn} \\ R_{xn+1} \\ R_{y1} \\ R_{y2} \\ \ldots \\ R_{yn} \\ R_{yn+1} \\ R_{z1} \\ R_{z2} \\ \ldots \\ R_{zn} \\ R_{zn+1} \end{pmatrix} = \begin{pmatrix} D_{x1} \\ D_{x2} \\ \ldots \\ D_{xn} \\ D_{y1} \\ D_{y2} \\ \ldots \\ D_{yn} \\ D_{z1} - W \\ D_{z2} - W \\ \ldots \\ D_{zn} - W \\ F_{y0} \\ h \\ 0 \end{pmatrix}$$

Fig. 20. Matrix representation of the 3D problem

Computing several cases, it is possible to highlight the fact that a transformation which is composed of two rotations (one around $\overrightarrow{u_x}$ and the other one around $\overrightarrow{u_y}$) can be used to transform the problem into a 2D problem. Therefore, an analytical solution can also be found in the 3D case and the problem seems to be entirely solved.

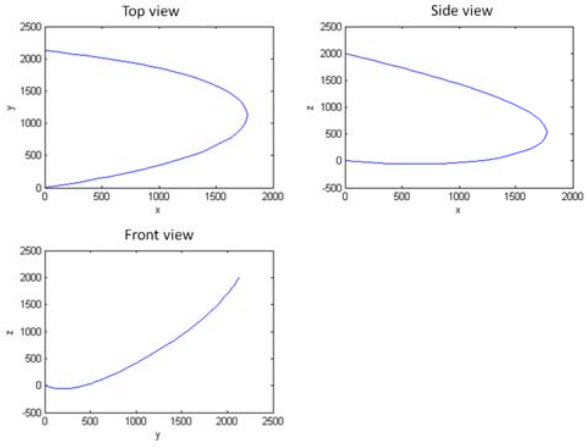


Fig. 21. 3-view of the shape of the cable

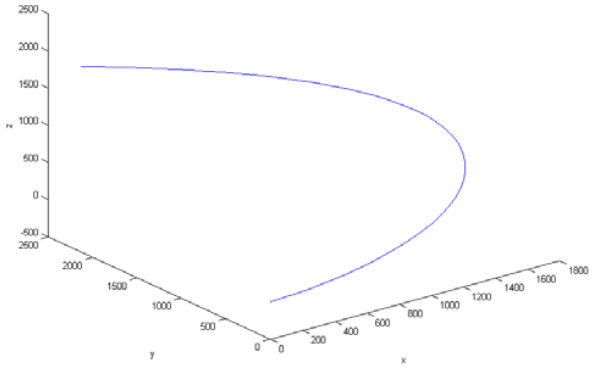

Fig. 22. 3D-visualization of the shape of the cable

### B. Possible Transformations

Since an accurate analytical solution has been found for a 2D configuration, the goal is to find a plan that contains the cable so that a 2D resolution can be performed analytically and the 3D solution could be determined with rotations. Thus, a first rotation is applied around $\overrightarrow{u_x}$ and the corresponding matrix is $R_x$ and is defined by (48).

$$R_x = \begin{pmatrix} 1 & 0 & 0 \\ 0 & \sqrt{1 - \frac{z_f^2}{z_f^2+y_f^2}} & \frac{z_f}{\sqrt{z_f^2+y_f^2}} \\ 0 & -\frac{z_f}{\sqrt{z_f^2+y_f^2}} & \sqrt{1 - \frac{z_f^2}{z_f^2+y_f^2}} \end{pmatrix} \tag{48}$$

Another rotation around $\overrightarrow{u_y}$ using $R_y$ defined by (49) is also performed and the result is displayed in Fig. 23.

$$R_y = \begin{pmatrix} \sqrt{1 - \frac{z_m^2}{z_m^2+x_m^2}} & 0 & \frac{z_m}{\sqrt{z_m^2+x_m^2}} \\ 0 & 1 & 0 \\ -\frac{z_m}{\sqrt{z_m^2+x_m^2}} & 0 & \sqrt{1 - \frac{z_m^2}{z_m^2+x_m^2}} \end{pmatrix} \tag{49}$$

It can be concluded that, even if the cable is not perfectly in the plane, the distance between the cable and the curve is

lower than 10 cm which is negligible compared to the cable length equal to several kilometers.

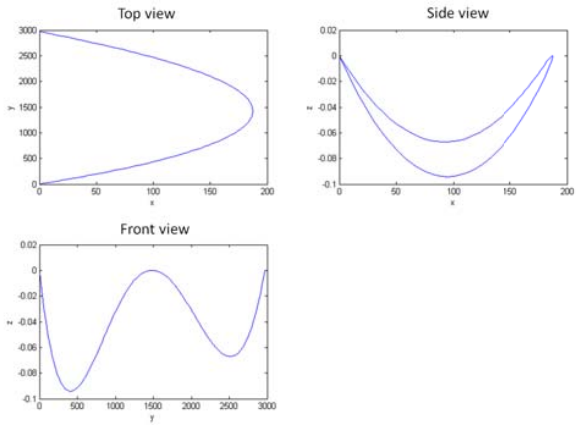


Fig. 23. Cable after a double rotation

## X. Conclusion

The goal of this project was to study the characteristics and the shape of the cable used to link the turbine and the aircraft in the new "Jet-stream Airsail" concept. The latter would be able to cross the Atlantic Ocean without consuming fuel. The first step was to model the drag coefficient of the cable. Since a circular cross-section creates an important drag, it has been found more profitable to streamline the cable and its optimal shape has been determined as well as its corresponding aerodynamic characteristics. In order to compute the exact drag along the cable, the jet-stream has been modeled as well as the atmospheric properties such as the density. The second step was the numerical computation of the shape of the cable by discretizing it and applying the Newton's second law and the boundary conditions. The software `Matlab` was used and has provided a useful framework to compute and display the results. The analysis of the results shows physical limitations which would be important to consider for the design and the optimization of the concept. To check the accuracy of the code, it has been compared to analytical solutions under specific and simplified conditions. The third step was to find an analytical solution of this problem. Since there were too many parameters and dependence between each other, a sensitivity analysis was performed and unessential factors was neglected or simplified. Then, a complete analytical solution has been derived and would highly accelerate the process and enable trade-off studies during the design process. Even if it has been simplified, the model is relatively precise since the relative error is around 15% in the worst cases and around several percents for typical values and nominal cases. Finally, a 3D approach was proposed to solve more complex problems with lateral forces. It has been shown that a combination of two rotations would allow the use of analytical solutions, even with lateral forces.

This study was performed in cruise and steady-state conditions but it would be useful to study more complex flying conditions such as gusts, climb and descent phases as well as turn. Another problem remains the take-off and landing phases and should also be considered in the next design steps.

## Acknowledgment

The authors would like to thank Jean-Luc Boiffier and Clément Toussaint from the French Aerospace Laboratory (ONERA) for their help and support.

## References

[1] C. H. Gibbs-Smith. *Clément Ader: his flight-claims and his place in history*. Her Majesty Stationary Office, 1968.
[2] Clement Toussaint. Jet-stream airsail. European Project Proposal.
[3] R. Johnstone. Condor-high altitude long endurance (hale) automatically piloted vehicle (apv). In *AIAA Paper*, 1990.
[4] A. Goo, N. Arntz, and R. Murphy. Condor for high altitudes. *Aerospace America*, 27(2):36–37, 1989.
[5] B. Henderson. Boeing condor raises uav performance levels. Technical report, Aviation Week & Space Technology, April 1990.
[6] M. Dornheim. Perseus high altitude drone to probe stratosphere for sst feasibility studies. Technical report, Aviation Week & Space Technology, 1991.
[7] G. Taubes. Nasa launches a 5-year plan to clone drones. *Science*, 260:286, April 1993.
[8] Anon. Strato 2c bringt europas klimaforschung weiter voran. *BundesMinisterium fur Forschung und Technologic (BMFT) Journal*, 5:11, October 1992.
[9] H. Kunkler. Antrieb der strato 2cintegraler bestandtteil einer systemlosung. Technical Report 17, Zeitschrift fur Flugwissenschaften und Weltraumforschung, 1993.
[10] Wubbo J.Ockels. The flying dutchman project, January 2005.
[11] J. Melkert. *STRATOW First Model Calculations and Tests*. PhD thesis, Delft University of Technology, July 1992.
[12] P. Rebuffet. *Aérodynamique expérimentale*. Number v. 1; v. 3. Dunod, 1969.
[13] Jack Moran. *An Introduction to Theoretical and Computational Aerodynamics*. Courier Dover Publications, 1984.
[14] Nathalie Bivaud. Le choix d'un profil pour optimiser les performances avion. Master's thesis, ESMA/ONERA/SUPAERO, 1998.
[15] Robert E. Sheldahl and Paul C. Klimas. Aerodynamic characteristics of seven symmetrical airfoil sections through 180-degree angle of attack for use in aerodynamic analysis of vertical axis wind turbines. Technical report, Sandia National Laboratories, 1981.
[16] Alfred L. C. Roelen Wubbo J. Ockels, Joris A. Melkert. Stratospheric towed vehicle concept. *Journal of Aircraft*, 31(6):1328–1332, 1994.